Video Article

Lens-free Video Microscopy for the Dynamic and Quantitative Analysis of Adherent Cell Culture

Cedric Allier[1], Romaric Vincent[1], Fabrice Navarro[2], Mathilde Menneteau[2], Lamya Ghenim[3,4], Xavier Gidrol[3], Thomas Bordy[1], Lionel Hervé[1], Olivier Cioni[1], Sabine Bardin[5], Michel Bornens[5], Yves Usson[4,6], Sophie Morales[1]

[1]CEA, LETI, DTBS, LISA, Université Grenoble Alpes

[2]CEA, LETI, DTBS, LBAM, Université Grenoble Alpes

[3]CEA, INSERM, BIG, Université Grenoble Alpes

[4]CNRS, FR CNRS 3425

[5]CNRS, UMR 144, Molecular Mechanisms of Intracellular Transport, PSL Research University, Institut Curie

[6]TIMC-IMAG

Correspondence to: Cedric Allier at cedric.allier@cea.fr

URL: https://www.jove.com/video/56580
DOI: doi:10.3791/56580

Keywords: Lens-free microscopy, video cytometry, dense cell cultures, quantitative microscopy

Date Published: 11/27/2017

Citation: Allier, C., Vincent, R., Navarro, F., Menneteau, M., Ghenim, L., Gidrol, X., Bordy, T., Hervé, L., Cioni, O., Bardin, S., Bornens, M., Usson, Y., Morales, S. Lens-free Video Microscopy for the Dynamic and Quantitative Analysis of Adherent Cell Culture. *J. Vis. Exp.* (), e56580, doi:10.3791/56580 (2017).

Abstract

Here, we demonstrate that lens-free video microscopy enables us to simultaneously capture the kinetics of thousands of cells directly inside the incubator and that it is possible to monitor and quantify single cells along several cell cycles. We describe the full protocol used to monitor and quantify a HeLa cell culture for 2.7 days. First, cell culture acquisition is performed with a lens-free video microscope, and then the data is analyzed following a four-step process: multi-wavelength holographic reconstruction, cell-tracking, cell segmentation and cell division detection algorithms. As a result, we show that it is possible to gather a dataset featuring more than 10,000 cell cycle tracks and more than $2x10^6$ cell morphological measurements.

Video Link

The video component of this article can be found at https://www.jove.com/video/56580/

Introduction

Monitoring cultured mammalian cells throughout several cell cycles and measuring accurately cell size and cell dry mass is a challenging task. Several label-free optical techniques are able to perform this task[1,2]: phase-shifting interferometry[3], digital holographic microscopy (DHM)[4,5,6,7], quadriwave lateral shearing interferometry[8,9] and quantitative phase tomography[10,11]. These methods have led to many new insights into the understanding of the cell cycle of mammalian cells. However they are seldom coupled with automatic cell tracking algorithms and their throughput remains limited when measuring cell mass trajectories[1] (N<20 in respectively[3,4,5,6]). Hence a novel optical method is needed to measure cell mass trajectories with large statistics (N>1000).

In this paper, we demonstrate the capability of lens-free video microscopy to simultaneously image thousands of cells directly inside the incubator, and then quantify single cell metrics along thousands of individual cell cycle tracks. Lens-free microscopy is a quantitative phase imaging technique which allows the acquisition of phase image of densely packed cells over a very large field of view (typically several tens of mm^2, here 29.4 mm^2)[12,13,14,15]. Several metrics at the single cell level are determined, *e.g.*, cell area, cell dry mass, cell thickness, cell major axis length and cell aspect ratio[12,15], from each image. Then, by applying a cell-tracking algorithm, these features can be plotted for every single cell as a function of the experiment time[14,15]. Furthermore, by detecting the occurrence of cell divisions in the cell tracks, it is possible to extract other important information such as the initial cell dry mass (just after the cell division), the final cell dry mass (just before the cell division) and the cell cycle duration, *i.e.*, the time between two consecutive divisions[15]. All these measurements can be computed with very good statistics (N>1000) since the large field of view would typically allow the analysis of 200 to 10,000 cells in a single lens-free acquisition.

In order to explain this methodology based on lens-free video microscopy, we describe the protocol to monitor and quantify a HeLa cell culture for 2.7 days. Data analysis is a four-step process based on multi-wavelength holographic reconstruction, cell-tracking, cell segmentation and cell division algorithms. Here it is shown that the spatial resolution and the relatively fast frame rate (one acquisition every 10 minutes) obtained with this lens-free video microscopy setup is compatible with standard cell-tracking algorithms. The full analysis of this dataset results in the measurement of 10,584 cell tracks over complete cell cycles.

To summarize, lens-free video microscopy is a powerful tool to automatically monitor thousands of unlabeled, unsynchronized, and unmodified cells per experiment; each cell being tracked over several cell cycles. Our measurements thus provide the mean value of several cell parameters, but more importantly, the inter-cell variability over a large population of cells.

Protocol

1. Cell culture monitoring acquisition

1. Grow HeLa cells in DMEM + glutamine (e.g., GlutaMAX) medium supplemented with 10% (v/v) heat-inactivated fetal calf serum and 1% penicillin and streptomycin.
2. Coat 6-well glass bottom culture plates with fibronectin (25 µg/mL) for 1 h. Then seed $2x10^4$ cells per well.
3. During the acquisition, change the medium every 3 days.
4. For the time-lapse acquisition, use the video lens-free microscope (commercially available).
   NOTE: This is based on the lens-free computational imaging technique as described by Ozcan *et al.*[16] which was modified to perform continuous monitoring in an incubator at a controlled temperature of 37 °C[12,15]. It features a complementary metal oxide semiconductor (CMOS) image sensor with a pixel pitch of 1.67 µm and an imaging area of 6.4 x 4.6 mm^2. Multiple wavelength illumination is provided by a multichip light emitting diode (LEDs) device, which delivers red, green and blue illumination. The wavelengths are centered, on 636, 521, and 452 nm respectively, with a spectral bandwidth of 25, 45, and 25 nm respectively. The red-green-blue (RGB) LEDs are located above a 150-µm pinhole at a distance of approximately 5 cm from the cells. The light power measured close to the LED is as low as 10 µW at each wavelength and the illumination time is only one second per acquisition. Hence, no photo-toxicity problems are expected when cell cultures are observed under the lens-free video microscope.
5. Put the cell culture container put in contact with the CMOS sensor (**Figure 1**). Use a container with a glass coverslip at the bottom, which is important for the quality of the lens-free acquisition. Plastic containers can also be used but the lens-free acquisition will be degraded owing to the poor optical quality of these containers.
6. Control the video lens-free microscope with the acquisition software (commercially available), which performs both the time-lapse acquisition and the holographic reconstruction. The parameters that need to be entered by the user in the software interface are the frame rate, the duration of the experiment, and the type of cell culture, i.e. adherent cells or floating cells.
7. Set the input parameters of the acquisition software. Set the frame rate set to one acquisition every 10 minutes and set the cell culture type to 'adherent'.
   NOTE: A frame rate of one acquisition every 10 minutes is a good compromise as it ensures a reliable cell tracking while the size of the resulting dataset to be analyzed is still reasonable. The fastest frame rate achievable with this lens-free microscopy setup is one acquisition every 5 minutes. Further increasing the framerate results in excessive heating of the CMOS sensor which can affect the viability of the cells in culture.
8. Start the time-lapse acquisition, and the holographic reconstruction algorithm (commercially available) will automatically process the lens-free acquisition to obtain the phase image of the cell culture. The holographic reconstruction algorithm is based on a multi-wavelength phase retrieval algorithm[17] and provides an RGB reconstructed phase image in the range of [-π, +π] for each single cell over a large field of view of 29.4 mm^2. The principle of lens-free in-line holography is to illuminate a thin sample (at z=0) with a plane wave (of amplitude 1 after normalization) and to detect on a CMOS sensor the subsequent diffraction intensity image at a short distance z=Z, typically 1 mm after the sample. In our setup, the illumination is sequentially switched to 3 wavelengths (λ_1=0.450 µm, λ_2=0.540 µm, λ_3=0.647 µm) to measure three diffraction patterns of the same sample.

2. Cell culture data analysis

1. For cell-tracking, use the Trackmate algorithm, an open source Fiji plugin for the automated tracking of single particles [18]. At first, load the full time-lapse acquisition into Fiji (load image sequence command). Owing to the large size of the datasets, which features typically 400 RGB frames of 29.7 Mb, it is faster to load them in 8-bit format. Next the Trackmate Fiji plugin guides the user through several stages of the cell-tracking algorithm, namely a cell detection stage, a cell tracker stage and several filters applied to the cell detections and the computed tracks. At every stage, configure the algorithms and display the results immediately so that, if necessary, one can easily navigate back and forth to readjust the settings. The various menus of the Trackmate interface are shown in **Figure 2** with the actual settings used for the HeLa cells experiment.
2. Set the input parameters of the acquisition software as following (see **Figure 2**). Set the estimated blob diameter to 15 pixels, the detector threshold to 0.25, the linking maximum distance to 15 pixels, the gap-closing max distance to 15 pixels, and the number of spots in tracks to 3.5.
   NOTE: These settings will obviously differ from one experiment to another, especially the 'estimated blob diameter' which corresponds to the cell size (here given in pixels of 1.67 µm). The same remark applies to the 'linking max distance' which account for the maximum distance travelled by a cell within two consecutive frames (here given in pixels of 1.67 µm). Its optimal value would depend on cell motility but also on cell density.
3. At the end of the cell-tracking process, generate the results in the form of three text files ('Analysis' button, see **Figure 2**). The most useful file, named 'Spots in tracks statistics', consists of a table listing all detected cells with their respective (x,y) positions in the acquisition, their frame number and their track number. On the basis of this data, perform cell segmentation and detect cell divisions using dedicated algorithms (see supplementary code files). The two other files are named 'Links in tracks statistics' and 'Track statistics' and include all the results dealing with the tracks, *e.g.* track durations, number of detected gaps, track initial frame, etc.
4. Use the cell segmentation algorithm (see supplementary code file) to automatically extract several metrics describing the cell morphology from the reconstructed phase image. These metrics are the cell surface area (S), the cell major axis length (L), the cell minor axis length (l) and the cell aspect ratio (L/l).The phase recovered from lens-free microscopy is proportional to the density and thickness of the specimen layer as discussed previously[15].

5. In addition to the morphological features of the cell, extract quantitative cell dry mass (CDM) measurements from the reconstructed phase [13,19,20]

$$cell\ dry\ mass = \iint \frac{\lambda\varphi(x,y)}{2\pi\alpha}\delta x\delta y$$ Eq. (1)

where φ(x,y) is the reconstructed phase shift [19], λ the wavelength and α = 1.8 x 10^{-4} m^3/kg the specific refractive index which relates the variation of refractive index to dry mass [1,19].

6. Evaluate the cell thickness using an estimation of the difference between the cell refractive index and that of the culture media. The relation between the cell thickness *h*(*x*,*y*) and the measured phase shift is given by [20]:

$$n_{cell}(x,y) = n_{medium}(x,y) + \frac{\varphi(x,y)\lambda}{2\pi h(x,y)}$$ Eq. (2.1)

$$h(x,y) = \frac{\varphi(x,y)\lambda}{2\pi\Delta n(x,y)}$$ Eq. (2.2)

with $\Delta n(x,y) = n_{cell}(x,y) - n_{medium}(x,y)$, the refractive index difference between the cell and the culture media. In the following, assume a constant value of $\Delta n = 0.025$, which is estimated from the refractive index measured in HeLa cell nuclei (n=1.355[11]) and that of phosphate-buffered saline (PBS) culture media (n=1.33). Although the cell thickness value is only indicative as it is based on an assumption, its relative variations are meaningful and can be exploited to detect dividing cells.

7. Use the dedicated algorithm (see supplementary code file) to detect the occurrence of cell divisions and then extract cell tracks that are associated to the detected cell divisions, In order to detect a cell division, cells with a measured thickness larger than 8 µm are first identified, then check whether a new cell appears closely in space and time. In this way, the detection of cell divisions relies on two robust criteria. Alternative and more elaborate methods for cell division detection can be applied to the lensfree time-lapse acquisition[21,22,23].

Representative Results

For the holographic reconstruction process, the light field is described by a scalar field *A* (where $A_z^\lambda(\vec{r})$ is the complex value of *A* on the plane at distance *z* from the sample, and lateral position $\vec{r}$ and at wavelength λ). Light propagation is modeled by the Huygens-Fresnel theory which provides a propagator kernel $h_Z^\lambda(\vec{r})$. Therefore, the field amplitude at the detector plane, A_z is related to the light amplitude A_0 by the following relation:

$A_Z^\lambda = A_0^\lambda * h_Z^\lambda$ i.e. $A_Z^\lambda(\vec{r}') = \int d\vec{r} A_0^\lambda(\vec{r}) h_Z^\lambda(\vec{r}'-\vec{r})$

with $h_Z^\lambda(\vec{r}) = \frac{1}{i\lambda Z} e^{i\pi\frac{r^2}{\lambda Z}}$, where *i* is the complex number (i^2=-1)

The intensity measurement is simply modeled by $I_Z^\lambda(\vec{r}) = \left|A_Z^\lambda\right|^2$. The purpose of the reconstruction algorithm is to find a 'good' field A_0, related to the observed sample, which diffraction would match the measured intensity I_z. The strategy is to consider the amplitude field phase at the detector plane φ_z as unknown of the problem and to optimize a multispectral total variation criterion of the object. More explicitly, considering the fields

$$A_Z^\lambda(\vec{r},\varphi_Z) = \sqrt{I_Z^\lambda(\vec{r})}e^{i\varphi_Z^\lambda(\vec{r})}$$

$A_0^\lambda(\vec{r},\phi_z) = A_Z^\lambda(\vec{r},\phi_z) * h_{-Z}^\lambda$ i.e. $A_0^\lambda(\vec{r},\varphi_Z) = \int d\vec{r}' \sqrt{I_Z^\lambda(\vec{r}')} e^{i\varphi_Z^\lambda(\vec{r}')} . h_{-Z}^\lambda(\vec{r}-\vec{r}')$

for any phase field φ_z, $A_Z^\lambda(\vec{r},\varphi_Z)$ perfectly matches the data since $\left|A_Z^\lambda\right|^2 = I_Z^\lambda(\vec{r})$. So that the subsequent field $A_0^\lambda(\vec{r},\phi_Z)$ is a possible amplitude field in the sample plane, given the observed intensity image. This is the reason why a criterion on A_0 is used to specify a unique solution among all data-matching possibilities. The criterion to minimize was chosen as:

$$\varepsilon(\varphi_Z) = \int \sqrt{\sum_\lambda \left|\frac{\partial}{\partial x}A_0^\lambda\right|^2 + \left|\frac{\partial}{\partial y}A_0^\lambda\right|^2}$$

where x and y are the coordinates for the plane, i.e. $\vec{r} = (x,y)$. Using such a criterion enables to select, among all possible fields, a sample field displaying sharp edges at the same position for all wavelengths, which is physically meaningful. This method reduces the occurrence of 'twin-images' in the reconstructed field A_0. The 'twin-image' is an important artefact that results from a lack of phase information during the acquisition process.

For the practical computation, the integrals are discretized with a spatial sampling corresponding to the detector resolution, the derivatives are replaced by Sobel operators and convolutions by the Huygens-Fresnel propagator h_Z^λ are performed by going to the Fourier space where $\widetilde{h}_Z^\lambda$ has a simple expression: $\widetilde{h}_z^\lambda(\vec{u}) = e^{-i\pi\lambda z\vec{u}^2}$. Minimization of the (real) criterion ε with respect to the (real) set variables $\varphi_Z(\vec{r})$ is tackled by using the non-linear conjugated gradient method, which requires the gradient of ε to be computed for any phase associated with each detector pixels for each wavelength.

Cell reconstruction/Phase unwrapping

Figure 3 shows the results of the holographic reconstruction of one frame of a time-lapse acquisition of HeLa cells in culture. **Figure 3a** shows the full field of view of a raw acquisition in the blue channel on a 29.4 mm^2 area. Based on this image and the ones acquired in the red and green channels, the holographic reconstruction produces a RGB phase image of the cells as shown in **Figures 3b** and **3c**. The reconstructed phase image exhibits locally wrapped phase artefacts corresponding to cells that induce a phase shift exceeding +π. In order to perform a simple phase unwrapping, we implemented a heuristic mean, namely we detect the pixels with the value $\left|\frac{\varphi_{blue}}{\varphi_{red}} - 1\right|$ exceeding 0.3 and set these pixels to +π.

This simple method is based on a property of the RGB reconstructed phase images. In theory at each pixel we should measure a ratio $\frac{\varphi_{blue}}{\varphi_{red}}$ equal to $\frac{\lambda_{red}}{\lambda_{blue}}$. But in the case of mitotic cell, when phase wrapping occurs, this relationship is no longer maintained in the RGB reconstructed phase image (**Figure 3f**). The above mentioned heuristic method takes advantage of this property, so that a simple thresholding can be used to detect the pixels presenting phase wrapping. The results of the reconstructed phase image before and after unwrapping is shown in **Figures 3f** and **3g**, respectively. These unwrapped phase images are then fed into the cell-tracking algorithm. Without this unwrapping step, the cell-tracking algorithm would fail to detect cells in division and cells of large thickness, which would compromise the final results. The resolution of the reconstructed phase image was estimated to be approximately 5 µm[15] (full-pitch spatial resolution), which is relatively coarse. It is nonetheless possible to observe details such as lamellipodia and cell cytoplasm (**Figures 3f and 3g**). Most importantly, the image obtained by lens-free microscopy displays a large contrast and is exempt of halo artefacts. This facilitates automatic cell detection and cell-tracking.

Cell culture data analysis

To extract the cell cycle tracks, the data analysis relies on a series of different algorithms, namely the cell tracking performed with the Trackmate Fiji plugin, the detection of divisions and ultimately the extraction of cell cycle tracks, *i.e.* the sequence in between two cell divisions. In the following we discuss the quality of the outputs of these algorithms when compared to manual measurements.

Figure 4 shows different screen captures of the cell-tracking results, the results of the cell detection algorithm and the results of the cell-tracking analysis. The detection of cells in the lens-free acquisition (**Figures 4a-4c**) is the first step of the cell-tracking algorithm. In order to validate the cell detection algorithm, we annotated manually a small portion of the time-lapse lens-free acquisition (214 frames of 663 x 663 $µm^2$). We manually selected a total of 5365 cell positions and compared these results with those obtained by the Trackmate Fiji plugin. **Figure 5** shows the results in terms of true detection, false positives and false negatives. The resulting sensitivity is about 96% and the positive predictive value as large as 99.7%. These high values reflect the good quality of the reconstructed phase images obtained with the lens-free video microscopy setup. After cell detection, a cell segmentation algorithm allows to measure - for each cell - several different metrics, *e.g.* the cell area, the cell dry mass and the cell thickness. **Figure 6a** depicts the principle of the segmentation algorithm and **Figure 6f** shows segmented images in a time sequence for a region of interest of 663x663 $µm^2$ (the same as in **Figure 5**). The algorithm initiates the segmentation by thresholding the phase image (see **Figure 6b**) and then it applies a seeding procedure (see **Figure 6c**). Namely the pixels of the center of the detected cells are set to the value of the corresponding track. The X-Y positions of the cells and their corresponding track number are provided by the 'Spots in tracks statistics' file obtained after cell tracking. Then, an iterative filling procedure is implemented that extends the seed to the boundaries of the cell (**Figures 6c-6e**) determined by the initial thresholding (**Figure 6b**). This filling procedure relies on basic operations in mathematical morphology, *e.g.,* dilation and erosion. From the segmentation result, it is then possible to calculate several metrics at the single cell level, *i.e.* morphological features like the cell length, the cell area and the cell aspect ratio, but also, more importantly, the cell dry mass according to Eq. 1. In order to assess the reliability of the lens-free microscopy measurement of the cell dry mass, we have compared the lens-free reconstructed phase image of fixed HeLa cells (**Figure 6g**) with the same region acquired by means of a digital holographic microscopy with a 5X objective (**Figure 6h**). **Figure 6i** shows the cell dry mass measured by mean of lens-free microscopy as a function of the dry mass measured with DHM for 302 segmented HeLa cells. There is a good correlation between the two measurements (coefficient of determination R^2 is 0.86, slope = 0.9, offset = -17 pg). From **Figure 6i**, we can estimate the precision of the cell dry mass measurement obtained by means of lens-free microscopy. The precision, measured as the mean square error between the lens-free data and the linear fit, is about 16 pg.

When compiling all single cell measurements over the full time-lapse acquisition, it is then possible to obtain scatterplots of several metrics as a function of time as shown in **Figure 7**. These scatterplots provide information on the kinetics of the cultured cells over a very large population. The number of cells in the field of view increases from 2000 up to 15000 (**Figure 7a**). Multiplied by the number of time points, this leads to a large dataset of $2.2x10^6$ detected cells, each of them characterized by its coordinates and morphological features, i.e. cell dry mass (**Figure 7b**), cell area (**Figure 7c**), cell average thickness (**Figure 7d**), major axis length (**Figure 7e**), and aspect ratio (**Figure 7f**).

Importantly, the combination of cell tracking and cell segmentation algorithms enables us to measure the kinetics at the single cell level. As an example, **Figure 8** shows the analysis of a cell track lasting about 66 hours and exhibiting four cell divisions at T0+4.1 h, T0+20.5 h, T0+36.7 h and T0+53.3 h. **Figure 8a** show the results of the automatic cell segmentation algorithm which allows us to delineate efficiently the surface of this cell. Using the cell segmentation, it is then possible to compute several metrics as a function of time, *e.g.* the cell surface area (**Figure 8b**), the cell dry mass (**Figure 8c**), the cell average thickness (**Figure 8d**) and the cell motility (**Figure 8e**). From these graphs, one can clearly measure the kinetics of these cellular metrics between cell divisions. In particular one can observe the increase of the cell area and dry mass during a cell cycle. In addition, using the automatic detection of cell divisions, three different cell cycle tracks can be extracted from this track and the cell cycle duration, i.e. the period in between two divisions, can be estimated. On the single cell track shown in **Figure 8**, we measured three cell cycle durations, namely 16.4 h, 16.2 h and 16.7 h. Compiling all the cell cycle tracks from the analysis of a 2.7 days time-lapse acquisition results in the detection of 16725 cell divisions and the description of 10,584 cell cycle tracks. It is then possible to measure the mean and the variability of the cell cycle duration with sound statistics. We found that the distribution of the cell cycle duration is close to Gaussian distribution (**Figure 9a**) with a mean of 16.5 h, and a relative standard deviation of 12.4% (standard deviation measured on the Gaussian peak divided by the mean of the distribution). The average doubling time of 16.5 h is consistent with the cell cycle lengths measured manually on the track presented on **Figure 8**. It lies however in the lower range of published values for HeLa doubling time which are usually between 20 and 30 h[24,25,26,27]. However, in ref.[28], a short doubling time of 16.2 ± 1.7 h is also mentioned. In order to further validate our measurements of cell cycle lengths and confirm the reliability of our lens-free microscopy technique, we have performed a manual tracking of 100 cell cycle tracks (10,148 cell positions). On the cell cycle tracks obtained manually (N=100) the measured cell cycle length is 16.7±1.9 h (N=100, **Figure 9b**). This is very close to the measurement of 16.5±2.1 h (N=10,584) obtained with the automatic cell tracking, demonstrating the validity of the overall analysis. When comparing the manual tracking of cell cycle trajectories to the one determined automatically, we found that 67% of the cell cycle tracks were successfully detected and that the cycle lengths measured automatically are well-correlated to the ones measured manually (**Figure 9b**). The detection efficiency of the cell cycle trajectories was measured in the first 32 hours of the experiment, at a density below 150 cells/mm^2. This detection rate obviously decreases with time, as the cell density increases up ~500 cells/mm^2. The number of detected cell cycle tracks reaches a plateau at T0+32 h (**Figure 9c**) while the number of cells still increases by a factor of three between T0+32 h and T0+72 h (**Figure 7a**). Considering the rate of false positive and negative detections, **Figure 9b** presents 5 outliers points: 4 of them are due to false negative detection (cycle length >25 h) and 1 to a false positive detection (cycle length <10 h). To obtain this results, we have used a high threshold on the thickness (8 µm) in the cell division detection algorithm, in order to favor a low false positive rate. In addition, the tracks presenting inconsistency have been filtered out, *i.e.* cell cycle which duration is below 6 h and tracks with a dry mass trajectory that does not increase linearly as a function of time. They are only 3% of the total number of cell cycle tracks. As a result, the distribution of cell cycle length obtained automatically is well-approximated by a Gaussian (**Figure 9a**) with a low number of short tracks (cell cycle length< 10 h, 5.1% of the total number of tracks) which would result from false positive division detections. Similarly, tracks displaying a long cell cycle, which would partially results from false negative division detections, are also rare (cell cycle length>25 h, 2.4% of the total number of tracks). Manual tracking of the cell cycle trajectories was also used to further assess the cell tracking performed with the plugin. We have measured on 6693 cells an overall localisation accuracy of 1.6 µm on matching points, which is within one pixel pitch (1.67 µm).

Other parameters can be examined, such as the cell initial dry mass (just after a division), the final dry mass (just before a cell division), as well as the average growth rate during the cell cycle. **Figure 9d** plots the initial and final cell dry masses as a function of time. It shows that both initial and final cell dry masses decrease with time. The median value of the initial cell dry mass decreases from 223 pg down to 130 pg and the final cell dry mass from 460 pg down to 220 pg. The ratio between the two remains stable at 1.89 ± 0.12 during the whole experiment (**Figure 9d-9e).** Finally, **Figure 9f** shows the evolution of the cell dry mass growth rate as a function of time over the 10,584 cell cycle tracks and we found that the decrease in cell growth rate is a common trend for the entire cell population in this particular experiment.

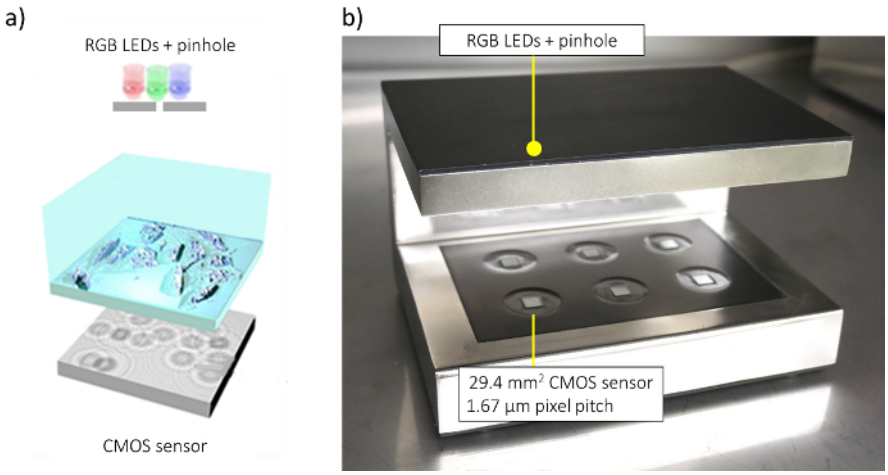

Figure 1. Lens-free microscopy. (a) Schematic of the lens-free microscopy acquisition setup. (b) Picture of the 6-wells lens-free video microscope. It uses a CMOS image sensor with a pixel pitch of 1.67 µm and an imaging area of 6.4 mm x 4.6 mm = 29.4 mm^2. Illumination is provided by a multi-colored RGB LEDs along with a pinhole placed at a distance of approximately 5 cm from the sample. Please click here to view a larger version of this figure.

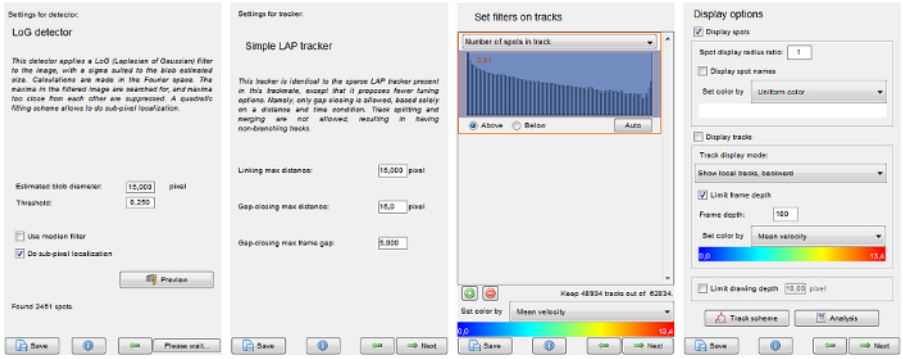

Figure 2. Trackmate interface. Main menus of the plugin shown with the actual settings used for the HeLa cell experiment. The estimated blob diameter was set to 15 pixels, the detector threshold was set to 0.25, the linking maximum distance was set to 15 pixels, the gap-closing max distance was set to 15 pixels, and the number of spots in tracks was set to 3.5. Please click here to view a larger version of this figure.

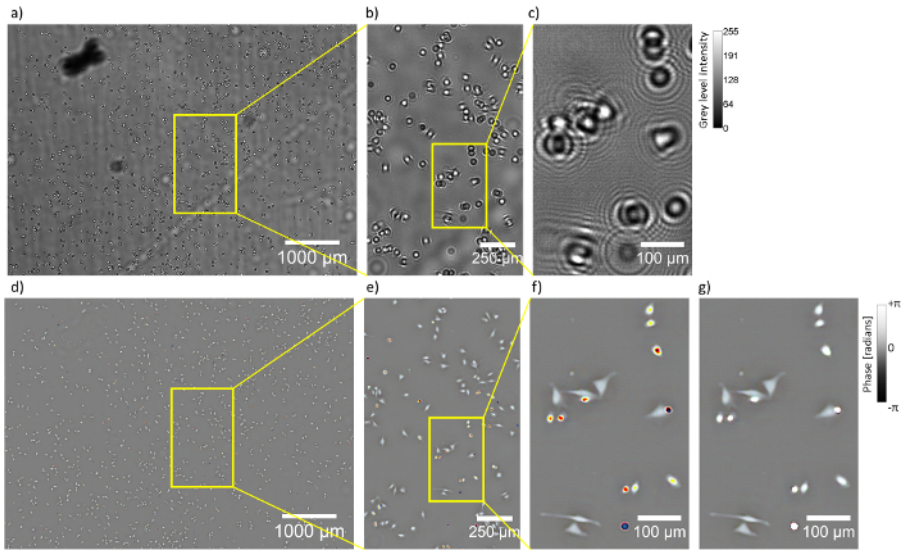

Figure 3. Holographic reconstruction process. (a) Raw acquisition of HeLa cells in culture by means of lens-free microscopy (full field of view of 29.4 mm^2). (b) Detail of (a). (c) Detail of (b). (d) RGB reconstructed phase image (full field of view of 29.4 mm^2). (e) Detail of (d). (f) Detail of (e). (g) Phase image obtained after phase unwrapping to be compared to (f), before unwrapping. Please click here to view a larger version of this figure.

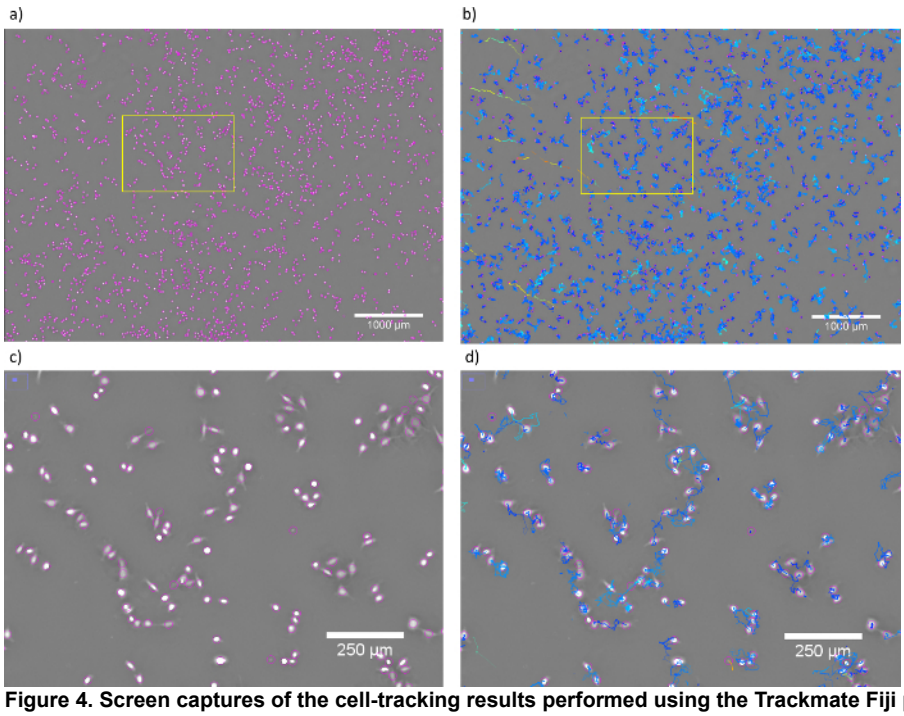

Figure 4. Screen captures of the cell-tracking results performed using the Trackmate Fiji plugin. (a) Results of the cell detection algorithm which is based on a Laplacian of Gaussian (LoG) detector. The picture shows the full field of view of the lens-free acquisition at T0+16h40min in which 2,451 cells are detected. The latter are surrounded with a purple circle. (b) Results of the cell-tracking algorithm. All cell tracks are shown over 50 frames (~8 hours) with a color code corresponding to the median velocity. (c, d) Detailed image of (a) and (b) respectively (yellow rectangle). Please click here to view a larger version of this figure.

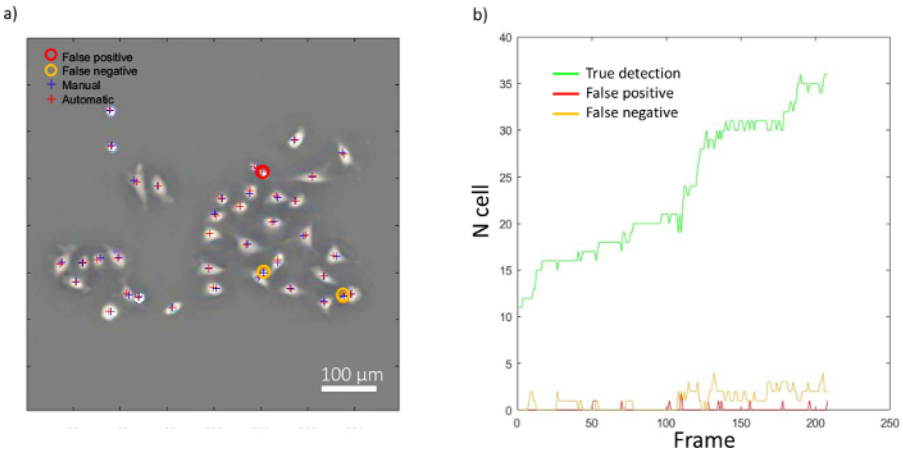

Figure 5. Validation of the cell detection stage of the cell-tracking algorithm. (a) Cropped image of HeLa cells in culture (663 x 663 µm^2) where the cell selected by hand are marked with blue crosses and those detected with the cell-tracking algorithm are marked with red crosses. This enables the determination of the false positive detection (red circle) and false negative detections (orange circle). (b) The rate of true detection (green line), false positive (red line) and false negative (orange) detection are plotted as a function of the experiment time. Please click here to view a larger version of this figure.

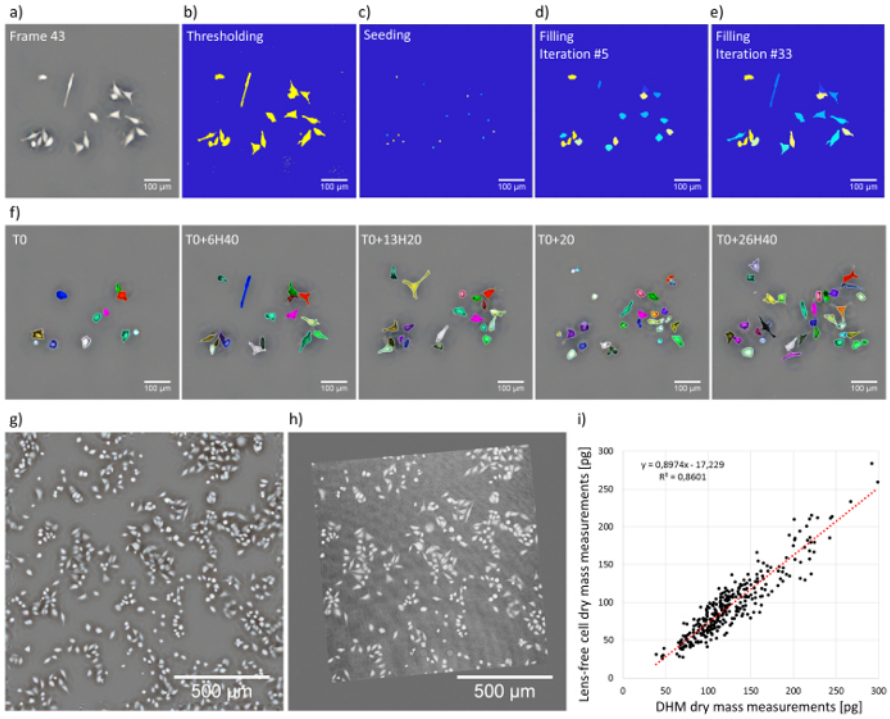

Figure 6. Results of the cell segmentation. (a) Reconstructed phase image of a region of interest of the time-lapse acquisition at T0+7 h (663 x 663 µm^2). (b) The algorithm initiates the segmentation by thresholding the phase image (c) The segmentation starts with a seeding procedure, i.e. the pixels of the centre of the detected cells are set to the value of the corresponding track. (d-e) Next and iteratively a filling procedure is implemented that extends the initial seeding to the boundaries of the cell determined by the initial thresholding (b). (f) The result of the segmentation algorithm is shown for a time sequence on a 663 x 663 µm^2 region (same as in **Figure 5**). The segmentation is shown as a colored surface overlaid on top of the reconstructed phase image. Note that the lens-free signal is mainly coming from the nuclear region, and the segmented areas fall close to the nucleus. (g) Reconstructed phase obtained by lens-free microscopy in fixed HeLa cells. This is a cropped image of the full field of view of 29.4 mm^2. (h) Phase image of the region shown in (g) obtained by digital holographic microscopy with a 5X objective (NA 0.12) illuminated with a laser at 647 nm. (i) Plot of the cell dry mass obtained by means of lens-free microscopy as a function of the dry mass measured by means of DHM. The scatterplot compiles 302 cells measurements. Please click here to view a larger version of this figure.

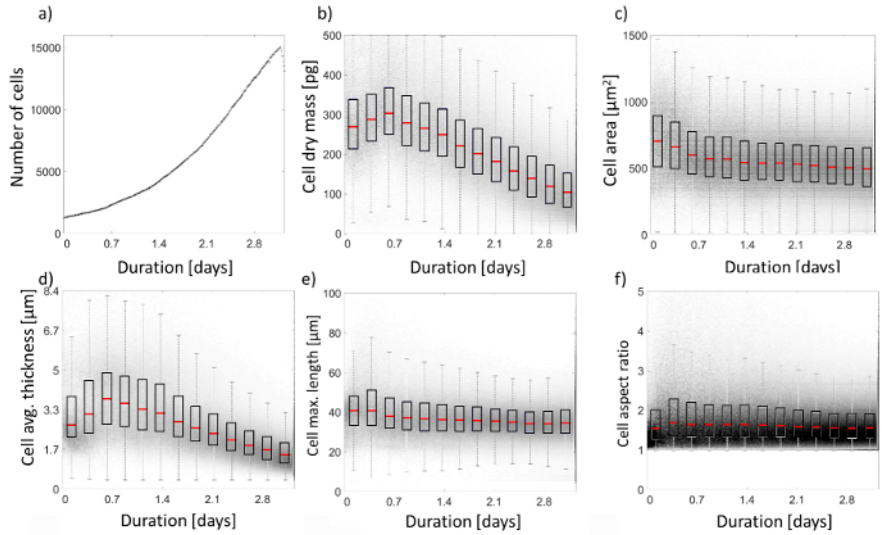

Figure 7. Data analysis of a 2.7-day lens-free time-lapse acquisition of HeLa cells. (a) Total number of cells counted in the full field of view of 29.4 mm^2 as a function of time. (b) Scatterplot of the cell dry mass as a function of time. On each box, corresponding to a bin of 6 hours, the red central mark indicates the median, and the bottom and top edges of the box indicate the 25th and 75th percentiles, respectively. The whiskers extend to the most extreme data points not considered outliers. (c-f) Scatterplots of the cell segmented area (c), the cell average thickness (d), the cell major axis length (e) and the cell aspect ratio (f) as a function of time. Please click here to view a larger version of this figure.

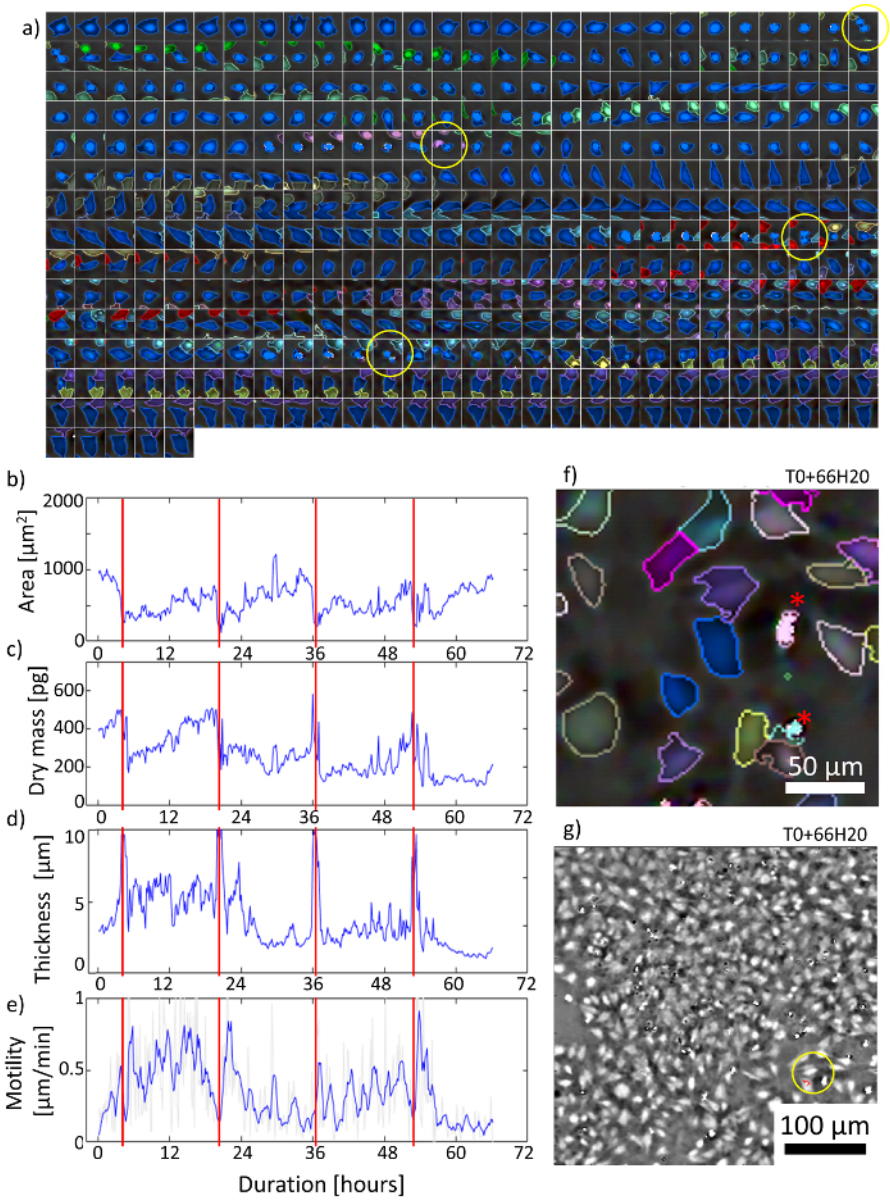

Figure 8. Data analysis of a 2.7-day cell trajectory (10 min frame interval). (a) Cell segmentation performed on the time-lapse acquisition of a cell track lasting about 66 h. The cell of interest is shown with a blue overlay. Each cropped image is 53 x 53 µm^2. The cell divisions are shown with yellow circles. (b) Plot of the cell area as a function of time. (c) Time evolution of the cell dry mass calculated from the integral of the phase over the segmented cell area according to Eq. (1). (d) Plot of the average cell thickness calculated as a function of time according to Eq. (2). The cell thickness exhibits sharp peaks corresponding to cell divisions (yellow circles in (a) and red lines in (b-c-d-e)). (e) Plot of the cell motility as a function of time. (f) Segmentation results corresponding to the last frame of the track at T0+66h20min when the cell density is about 475 cells/mm^2. The image is 200 x 200 µm^2 centered on the cell of interest. The white patches (red asterisks) correspond to cell debris that appear after one day of cell culture. (g) 800 x 800 µm^2 cropped reconstructed phase image of the last frame of this cell track. The cell of interest is surrounded by a yellow circle. Please click here to view a larger version of this figure.

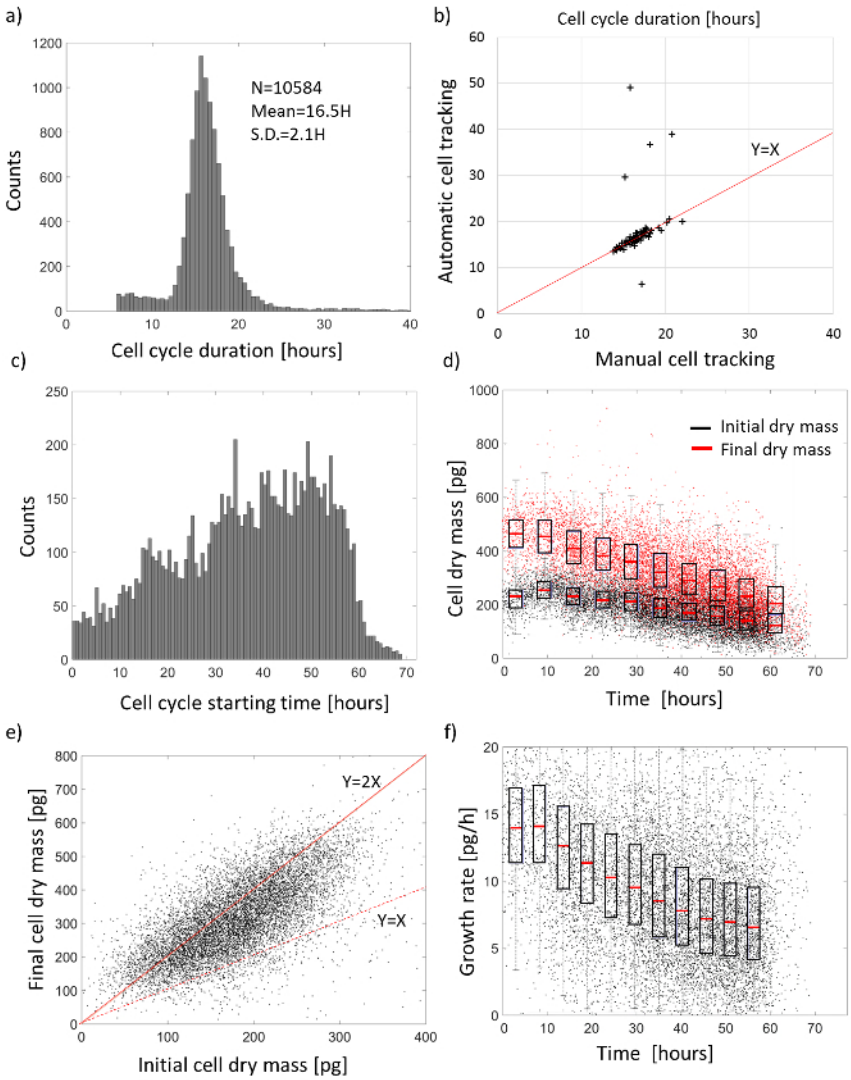

Figure 9. Cell cycle analysis. (a) Distribution of the cell cycle duration for a 2.7-day observation of cultured HeLa cells (N=10,584 cell cycles). The distribution of the cell cycle duration is close to a Gaussian with a mean of 16.5 hours and a relative standard deviation of 12.3% (standard deviation measured on the Gaussian peak divided by the mean of the distribution). (b) Comparison between the manual and automatic cell tracking for the determination of the cell cycle length. The manual tracking features 100 cell cycle trajectories (10,148 cell positions). (c) Distribution of the starting time of the automatically detected cell cycle trajectories. (d) Plot of the measured initial cell dry mass (just after cell division, black dots) and final cell dry mass (just before cell division, red dots) as a function of time. On each box, corresponding to a bin of 6 hours, the red central mark indicates the median, and the bottom and top edges of the box indicate the 25th and 75th percentiles, respectively. The whiskers extend to the most extreme data points not considered outliers. (e) Scatterplot of the final cell dry mass as a function of the initial dry mass. (f) Evolution of the cell dry mass growth rate as a function of the experiment time. Please click here to view a larger version of this figure.

Supplemental File 1. Code 'segmentation_from_trackmate_file_Version_Jove.m'
This Matlab code uses the 'trackmate' dataset to perform the cell segmentation of the complete time-lapse acquisition of which the reconstructed phase images are saved in the folder 'folder_out'. Please click here to download this file.

Supplemental File 2. Code 'lineage_Version_Jove.m'
This code uses the array 'trackmate' processed with the cell segmentation algorithm (segmentation_from_trackmate_file_Version_Jove.m), to extract the cell cycle trajectories and determine the different parameters of interest, *e.g.*, the cell cycle duration, the initial cell dry mass and the final cell dry mass. This code is in two parts, the first part deals with the detection of the dividing cells, and the second part with the analysis of the cell cycle trajectories. Please click here to download this file.

Discussion

In this paper, we show that lens-free video microscopy can be used inside an incubator to capture the kinetics of thousands of cells. In order to describe the overall methodology we explained how a 2.7-day time-lapse acquisition of HeLa cells in culture can be analyzed with standard cell-tracking algorithms. The result is a dataset featuring 2.2×10^6 cell measurements and 10,584 cell cycle tracks. The acquisitions were performed

on a culture of Hela cells with a relatively large cell-to-cell distance (cell density <500 cells/mm^2) and cell morphology that can be approximated with a disc. These two features facilitate the application of an automatic cell-tracking analysis which makes it possible to gather such a large dataset. Other cell lines with smaller cell-to-cell distance or with more complex morphologies would be more difficult to track and subsequent datasets would be smaller.

We believe that this approach is interesting for many studies, for instance for cell proliferation and cell size studies. The latter are an important area of research in fundamental biology and many questions remain unanswered as nicely discussed in a review by Ginzberg *et al.*[29]. The protocol proposed in this work provides thus a means to measure important metrics required for cell proliferation studies, i.e. the cell cycle duration, the cell dry mass, the cell dry mass ratio between the end and the start of the cycle and the cell dry mass growth rate. Besides the study of cell proliferation, this method will be of interest for the study of cell migration, since it can produce a large number of tracks, each one lasting several hours. The present protocol goes beyond the state of the art[14,30] by demonstrating for the first time the acquisition of thousands of cell tracks during more than 10 hours.

In conclusion, we have developed an easy-to-use lens-free technique that allows to track simultaneously thousands of label-free cells over several days of culture.

Disclosures

The authors have nothing to disclose.

Acknowledgements

The authors have nothing to acknowledge.

References

1. Zangle, T.A., Teitell, M.A. Live-cell mass profiling: an emerging approach in quantitative biophysics. *Nat Methods.* **11** (12), 1221-1228 (2014).
2. Popescu, G., Park, K., Mir, M., Bashir, R. New technologies for measuring single cell mass. *Lab Chip.* **14** (4), 646-652 (2014).
3. Reed, J. *et al.* Rapid, massively parallel single-cell drug response measurements via live cell interferometry. *Biophys J.* **101** (5), 1025-1031 (2011).
4. Mir, M. *et al.* Optical measurement of cycle-dependent cell growth. *Proc Natl Acad Sci. USA.* **108** (32), 13124-13129 (2011).
5. Girshovitz, P., Shaked, N.T. Generalized cell morphological parameters based on interferometric phase microscopy and their application to cell life cycle characterization. *Biomed Opt Express.* **3** (8), 1757-1773 (2012).
6. Kemper, B., Bauwens, A., Vollmer, A., Ketelhut, S., Langehanenberg, P. Label-free quantitative cell division monitoring of endothelial cells by digital holographic microscopy. *J Biomed Opt.*, **15** (3), 036009 1 -6 (2010).
7. Mir, M., Bergamaschi, A., Katzenellenbogen, B.S., Popescu, G. Highly sensitive quantitative imaging for monitoring single cancer cell growth kinetics and drug response. *PLoS One.* **9** (2), 1-8 (2014).
8. Bon, P., Savatier, J., Merlin, M., Wattellier, B., Monneret, S. Optical detection and measurement of living cell morphometric features with single-shot quantitative phase microscopy. *J Biomed Opt.* **17** (7), 076004 1-7 (2012).
9. Aknoun, S. *et al.* Living cell dry mass measurement usinq quantitative phase imaging with quadriwave lateral shearing interferometry: an accuracy and sensitivity discussion. *J Biomed Opt.* **20** (1), 1-4 (2015).
10. Cotte, Y. *et al.* Marker-free phase nanoscopy. *Nature Photonics.* **7** (2), 113-117 (2013).
11. Choi, W. *et al.* Tomographic phase microscopy. *Nat Methods.* **4** (9), 717-719 (2007).
12. Kesavan, S.V. *et al.* High-throughput monitoring of major cell functions by means of lensfree video microscopy. *Sci Rep.* **4**, 5942, 1-11 (2014).
13. Zheng, G., Lee, S.A., Antebi, Y., Elowitz, M.B., Yang, C. The ePetri dish, an on-chip cell imaging platform based on subpixel perspective sweeping microscopy (SPSM). *Proc Natl Acad Sci USA.* **108** (41), 16889-16894 (2011).
14. Pushkarsky, I., *et al.* Automated single-cell motility analysis on a chip using lensfree microscopy. *Sci Rep.* **4**, 4717 (2014).
15. Allier, C. et al. Imaging of dense cell cultures by multiwavelength lens-free video microscopy. *Cytom Part A.* **91** (5), 1-10 (2017).
16. Su, T-W., Seo, S., Erlinger, A., Ozcan, A. High-throughput lensfree imaging and characterization of a heterogeneous cell solution on a chip. *Biotechnol Bioeng.*, **102** (3), 856-868 (2009).
17. Delacroix, R. *et al.* Cerebrospinal fluid lens-free microscopy: a new tool for the laboratory diagnosis of meningitis. *Sci Rep.* **7**, 39893 (2017).
18. Tinevez, J.-Y. *et al.* TrackMate: an open and extensible platform for single-particle tracking. *Methods.* **115**, 80-90 (2016).
19. Popescu, G. Optical imaging of cell mass and growth dynamics. *Am J Physiol Physiol.* **295** (2), 538-544 (2008).
20. Liu, P.Y. *et al.* Cell refractive index for cell biology and disease diagnosis: past, present and future. *Lab Chip.* **16**, 634-644 (2016).
21. Rapoport, D.H., Becker, T., Mamlouk, A.M., Schicktanz, S., Kruse, C. A novel validation algorithm allows for automated cell tracking and the extraction of biologically meaningful parameters. *PLoS One.* **6** (11), e27315 (2011).
22. Al-Kofahi, O. *et al.* Automated cell lineage construction: A rapid method to analyze clonal development established with murine neural progenitor cells. *Cell Cycle.* **5** (3), 327-335 (2006).
23. Meijering, E., Dzyubachyk, O., Smal, I., van Cappellen, W.A. Tracking in cell and developmental biology. *Semin Cell Dev Biol.*, **20** (8), 894-902 (2009).
24. Posakony, J.W., England, J.M., Attardi, G. Mitochondrial growth and division during the cell cycle in HeLa cells. *J Cell Biol.*, **74** (2), 468-491 (1977).
25. Zocchi, E. *et al.* Expression of CD38 Increases Intracellular Calcium Concentration and Reduces Doubling Time in HeLa and 3T3 Cells. *J Biol Chem.* **273** (14), 8017-8024 (1979).
26. Reitzer, L. J., Wice, B. M., Kennell, D. Evidence that glutamine, not sugar, is the major energy source for cultured HeLa cells. *J Biol Chem.* **254** (8), 2669-2676 (1979).

27. Benedetti, A.D.E., Joshi-barve, S., Rinker-Schaeffer, C., Rhoads, R.E. Expression of Antisense RNA against Initiation Factor eIF-4E mRNA in HeLa Cells Results in Lengthened Cell Division Times, Diminished Translation Rates, and Reduced Levels of Both eIF-4E and the p220 Component of eIF-4F. *Mol Cell Biol.* **11** (11), 5435-5445 (1991).
28. Kumei, Y., Nakajima, T., Sato, A., Kamata, N., Enomoto, S. Reduction of G1 phase duration and enhancement of c-myc gene expression in HeLa cells at hypergravity. *J Cell Sci.* **93** (2), 221-226 (1989).
29. Ginzberg, M.B., Kafri, R., Kirschner, M. On being the right (cell) size. *Science.* **348** (6236), 1245075 (2015).
30. Mathieu, E. *et al.* Time-lapse lens-free imaging of cell migration in diverse physical microenvironments. *Lab Chip.* **16** (17), 3304-3316 (2016).

